Kovove Mater. 48 2010 291–300
DOI: 10.4149/km_2010_5_291

Unidirectional solidification of aluminium-nickel eutectic alloy

H. Kaya[1]*, U. Böyük[1], E. Çadırlı[2], N. Maraşlı[3]

[1] *Department of Science Education, Education Faculty, Erciyes University, Kayseri, Turkey*
[2] *Department of Physics, Faculty of Arts and Sciences, Niğde University, Niğde, Turkey*
[3] *Department of Physics, Faculty of Arts and Sciences, Erciyes University, Kayseri, Turkey*

Received 15 November 2009, received in revised form 3 June 2010, accepted 6 July 2010

Abstract

Aluminium-nickel of (99.99 %) high purity eutectic alloy was melted in a graphite crucible under vacuum atmosphere. The eutectic alloy was directionally solidified upward with a constant growth rate, V (8.32 μm s^{-1}) and different temperature gradients, G (0.83–4.02 K mm^{-1}) and also with a constant G (4.02 K mm^{-1}) and different V (8.32–483.25 μm s^{-1}) in the Bridgman type directional solidification furnace. The eutectic spacings, λ_i, have been measured from both transverse section (λ_T) and longitudinal section (λ_L, λ_m and λ_M) of the specimens. The undercooling values ΔT were obtained by using V and system parameters K_1, K_2. It was found that the values of λ_i decreased while V and G were increasing. The relationships between eutectic spacing λ_i and solidification parameters G and V were obtained by linear regression analysis. The dependence of eutectic spacings λ_i (λ_T, λ_L, λ_m and λ_M) on undercooling (ΔT) were also analysed. $\lambda^2 V$, $\Delta T\lambda$, $\Delta T V^{-0.5}$ and $\lambda^2 G$ values were determined by using λ_i, ΔT, V and G values. The results obtained in this work were compared with the Jackson-Hunt eutectic theory and similar experimental works.

K e y w o r d s: Al-Ni alloys, eutectic growth, eutectic spacing, undercooling

1. Introduction

Pure aluminium is soft and lacks strength, but alloyed with small amounts of copper, nickel, silicon, or other elements imparts a variety of useful properties. These alloys are of vital importance in the construction of modern aircraft and rockets. Aluminium-nickel alloy is one of the most important of these alloys. Eutectic alloys are the basis of most casting alloys. Research initially focused on materials for high temperature structural applications, but it was soon broadened to non-structural materials for electronic, magnetic, and optical applications [1]. The aluminium-nickel alloys centre on their potential as new high-temperature structural materials with high melting point, comparatively low density, good oxidation resistance and excellent high temperature mechanical properties. A major drawback of these materials is their room-temperature brittleness, which may be alleviated by controlling of the phase selection and microstructure, which would be directly affected by the kinetic process during solidification [1–7]. Solidification behaviour and structural characteristics of eutectic alloys in many systems continue to attract interest because of their influence on the properties and performance of materials containing eutectic constituents.

One of the most significant theoretical studies is the Jackson and Hunt (J-H) model of the eutectic structures [8]. The J-H model [8] gives the following relationship between the undercooling ΔT, the growth rate V and the eutectic spacing λ for an isothermal solidification front as:

$$\Delta T = K_1 V\lambda + K_2/\lambda, \tag{1}$$

$$\lambda_e^2 V = K_2/K_1, \tag{2a}$$

$$\Delta T\lambda = 2K_2, \tag{2b}$$

$$\frac{\Delta T^2}{V} = 4K_1K_2, \tag{2c}$$

where K_1 and K_2 can be calculated from the phase

*Corresponding author: tel.: +90 352 437 4901 # 37091; fax: +90 352 437 88 34; e-mail address: hasankaya@erciyes.edu.tr

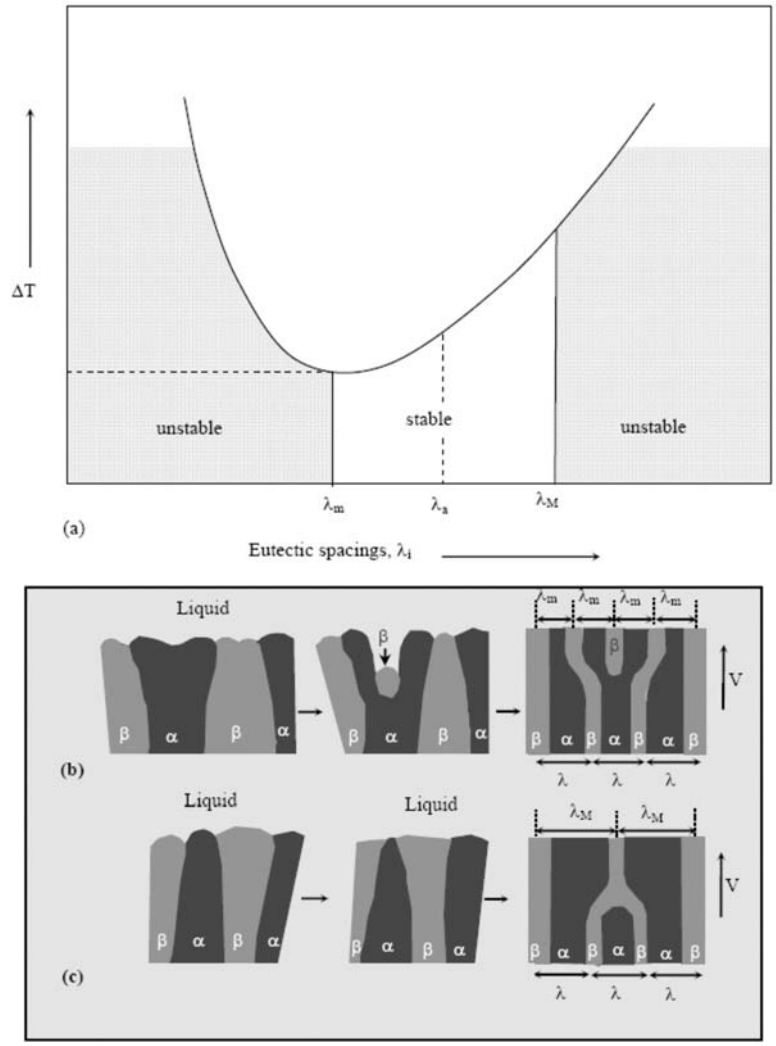

Fig. 1. (a) The schematic plot of average undercooling ΔT vs. eutectic spacing λ for a given growth rate V; the stable and unstable regions, as predicted by the Jackson-Hunt analysis, are also shown, (b) the readjustment of local spacing by positive terminations, (c) the readjustment of local spacing by negative terminations.

diagram and thermodynamic data. They are given by

$$K_1 = mPC_o/f_\alpha f_\beta D \tag{3}$$

and

$$K_2 = 2m\delta \sum_i (\Gamma_i \sin\theta_i/m_i f_i); \quad i = \alpha, \beta, \tag{4}$$

where $m = m_\alpha m_\beta/(m_\alpha + m_\beta)$, in which m_α and m_β are the slopes of the liquidus lines of the α and β phases at the eutectic temperature, C_o is the difference between the composition in the β and the α phase, f_α and f_β are the volume fractions of α and β phases, respectively. Γ_i is the Gibbs-Thompson coefficient, D is solute diffusion coefficient for the melt, θ_α and θ_β are the groove angles of α/liquid and β/liquid phases at the three-phase conjunction point. These parameters concerning Al-Ni eutectic alloy are given in the Appendix. The parameter δ is unity for the lamellar growth. For lamellar eutectic the parameter P is defined as [8]:

$$P = 0.3383(f_\alpha f_\beta)^{1.661}. \tag{5}$$

A well-known conjecture of this criterion is the minimum supercooling arguments. This indicates that the spacings λ_i, as indicated in Fig. 1, will be the operating point of spacing selection [9]. An analysis of the stability of the solidifying interface shows that this argument coincides with the marginal stability principle [10].

The solidification of eutectic alloys generally gives rise to lamellar or fibrous structures. The spacing of the lamellae or fibres is typically regular with dispersion around an average value. The experimentally confirmed inter-relationship between the eutectic spacings (λ_i), growth rate (V) and the undercooling (ΔT) in

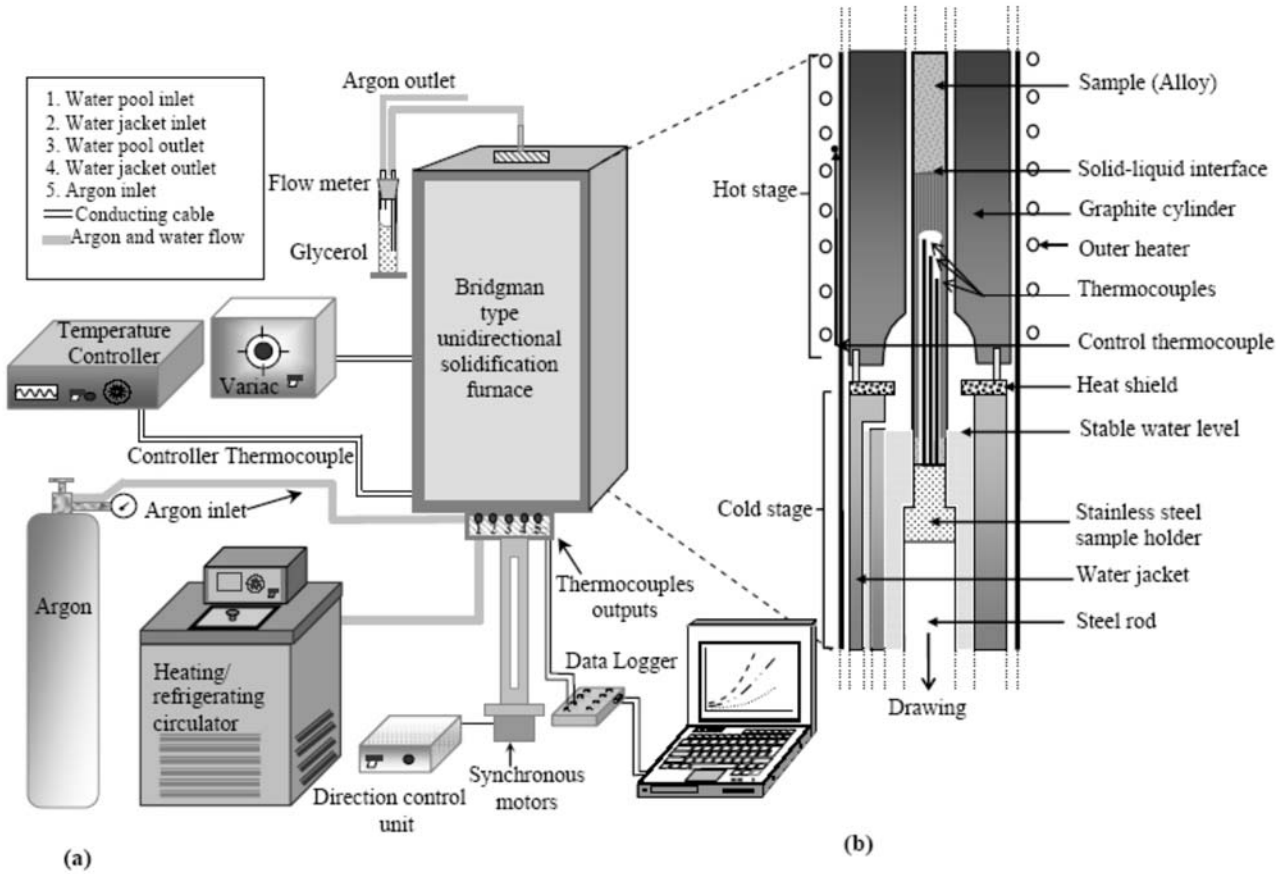

Fig. 2. (a) Block diagram of the experimental setup, b) the details of the Bridgman type directional solidification furnace.

eutectic system implies that the mechanism is available for changing the eutectic spacing when the growth rate and/or ΔT varied. Figure 1 shows the variation of the undercooling with eutectic spacing according to the minimum undercooling criterion. In Fig. 1a, λ_m is minimum eutectic spacing, λ_a is average eutectic spacing and λ_M is maximum eutectic spacing for the minimum undercooling condition. When λ_i becomes greater than λ_M, tip splitting occurs (Fig. 1b). When λ_i is smaller than λ_m, the growth will be unstable and overgrowth (Fig. 1c) will always occur [9]. So, eutectic spacings λ_i with steady state growth must satisfy $\lambda_m < \lambda_a < \lambda_M$ condition. For eutectic growth, the ΔT-V-λ relationships can be predicted by the Jackson-Hunt (J-H) [8] and Trivedi-Magnin-Kurz (TMK) [11] models. It is clear that the maximum spacing must be greater than twice the minimum spacing ($\lambda_M \geq 2\lambda_m$), otherwise the new lamella can not catch up [9].

Most studies [12, 13] have shown that eutectic terminations are constantly created and move through the structure during eutectic growth. The presence and movement of faults and fault lines provide a means by which eutectic spacing changes can occur in response to growth rate fluctuations or a small growth rate change. As can be seen from Fig. 1b,c, in this respect, the role of eutectic faults, and in particular eutectic terminations (positive and negative terminations), has been emphasised [13].

The aim of the present work is to experimentally investigate the dependence of the eutectic spacing λ_i on the temperature gradient (G), growth rate (V) and undercooling (ΔT) and also find out the effect of G and V on ΔT and to compare the results with the previous experimental results and the existing theoretical model.

2. Experimental procedure

2.1. Sample preparation and solidification

Al-5.7wt.%Ni eutectic samples were prepared by melting weighed quantities of Al and Ni of (> 99.9 %) high purity metals in a graphite crucible, which was placed into the vacuum melting furnace. The homogenized molten alloy was poured into 13 graphite crucibles (6.35 mm OD, 4 mm ID and 250 mm in length) in a hot filling furnace. Then, each specimen was positioned in a Bridgman type furnace in a graphite cylinder (40 mm OD, 10 mm ID and 300 mm in length). After stabilizing the thermal conditions in the furnace under an argon atmosphere, the speci-

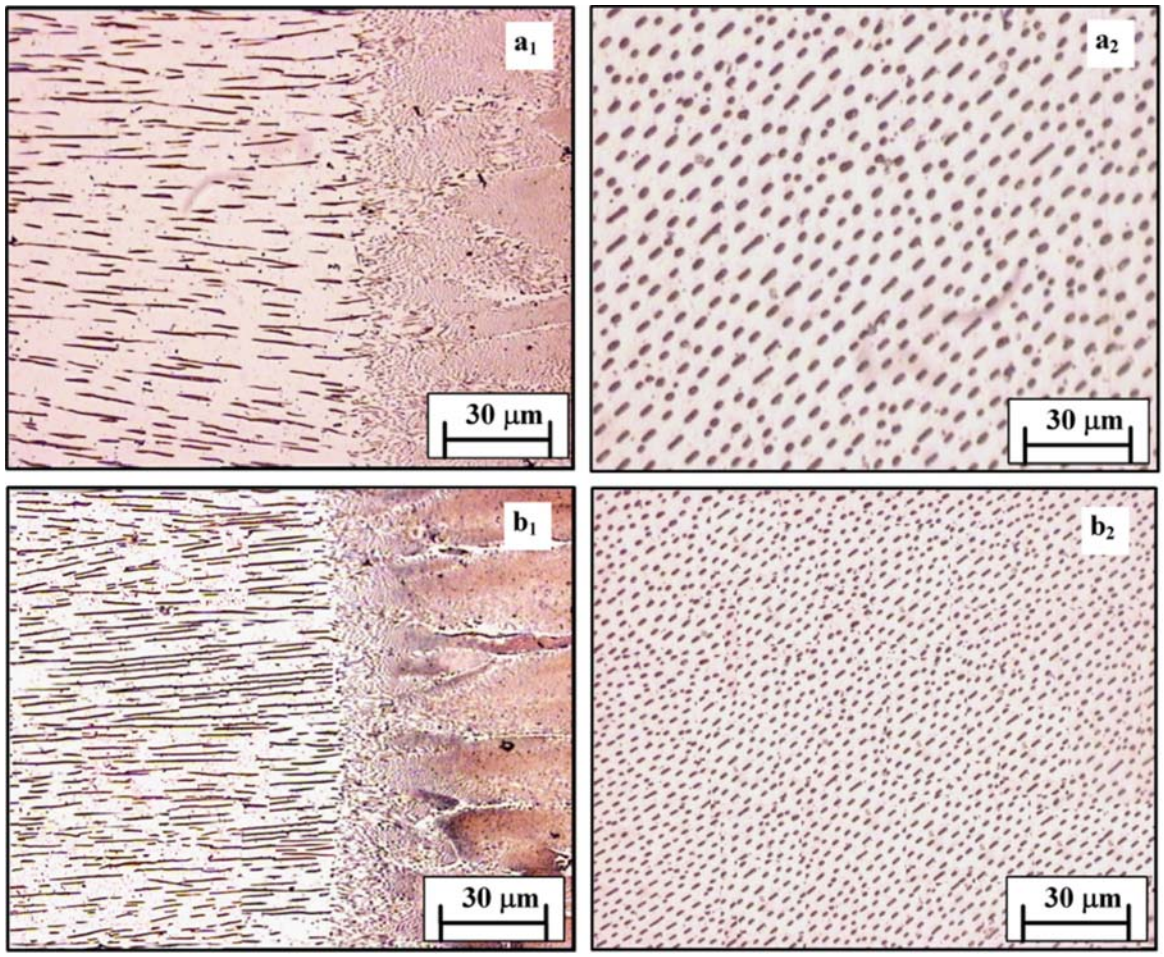

Fig. 3. Variation of eutectic spacings with growth parameters for directionally solidified Al-5.7wt.%Ni eutectic alloy: (a_1) longitudinal section, (a_2) transverse section ($G = 0.83\ \mathrm{K\ m^{-1}}$, $V = 8.32\ \mu\mathrm{m\ s^{-1}}$), ($b_1$) longitudinal section, (b_2) transverse section ($G = 4.02\ \mathrm{K\ mm^{-1}}$, $V = 483.25\ \mu\mathrm{m\ s^{-1}}$).

men was grown by pulling it downwards at various G (0.83–4.02 K mm^{-1}, V constant) and various V (8.32–483.25 μm s^{-1}, G constant) by means of synchronous motors. After approximately 100 mm steady state growth of the samples, they were quenched by pulling them rapidly into the water reservoir (see Fig. 2).

2.2. Metallographic process

The unidirectional grown and quenched specimens were removed from the graphite crucible and then ground to observe the solid-liquid interface and the longitudinal section, which included the quenched interface, was separated from the specimen. This part was ground, polished and etched to reveal the quenched interface. Furthermore, the longitudinal and transverse sections of the ground specimen were mounted in a cold-setting epoxy resin. The samples were wet ground down to grit 2500 and mechanically polished using 6, 3, 1 and 1/4 μm diamond paste. Finally the specimens were etched with an acid solution (75 ml H_2O, 10 ml HCl, 12 ml NHO_3 and 3 ml HF) to reveal the microstructure. The microstructures were photographed from both transverse and longitudinal sections by Olympus BH-2 type light optical microscope (Fig. 3).

2.3. Measurements of microstructural and growth parameters

The temperature in the specimen was measured with 0.25 mm in diameter K-type insulated three thermocouples fixed within the sample with spacing of 8–16 mm. All the thermocouple ends were then connected to the measurement unit consisting of data-logger and computer and the cooling rates were recorded with a data-logger via computer during the growth. When the solid/liquid interface was at the second thermocouple, the temperature difference between the thermocouples (ΔT) was read from data-logger record. The temperature gradient ($G = \Delta T/\Delta X$) for each sample was determined using the measured value of ΔT and the known value of ΔX.

The time taken for the solid-liquid interface passes

Table 1. Effect of temperature gradients G on the undercooling ΔT and the eutectic spacings λ_i at a constant growth rate V for the directionally solidified Al-Ni eutectic system, and the relationship between ΔT and G and also λ_i and G

Constant V, different G						
Solidification parameters			Microstructure parameters			
G ($\mathrm{K\,mm^{-1}}$)	V ($\mu\mathrm{m\,s^{-1}}$)	ΔT (K)	λ_T (μm)	λ_L (μm)	λ_m (μm)	λ_M (μm)
0.83	8.32	0.130	6.95 ± 0.12	7.90 ± 0.14	7.51 ± 0.16	8.30 ± 0.22
1.15	8.32	0.151	5.89 ± 0.14	6.87 ± 0.16	6.53 ± 0.13	7.21 ± 0.20
1.82	8.32	0.185	4.89 ± 0.13	5.50 ± 0.12	5.23 ± 0.11	5.78 ± 0.18
2.78	8.32	0.224	3.91 ± 0.07	4.34 ± 0.08	4.12 ± 0.07	4.56 ± 0.12
4.02	8.32	0.264	3.49 ± 0.12	3.89 ± 0.14	3.70 ± 0.09	4.08 ± 0.10
Relationships			Constant (k)		Correlation coefficients (r)	
$\Delta T = k_1\, G^{0.45}$			$k_1 = 0.142$ ($\mathrm{K^{0.55}\mu m^{0.45}}$)		$r_1 = 0.999$	
$\lambda_\mathrm{T} = k_2\, G^{-0.45}$			$k_2 = 0.30$ ($\mathrm{K^{0.45}\ \mu m^{0.55}}$)		$r_2 = -0.995$	
$\lambda_\mathrm{L} = k_3\, G^{-0.47}$			$k_3 = 0.27$ ($\mathrm{K^{0.47}\ \mu m^{0.53}}$)		$r_3 = -0.994$	
$\lambda_\mathrm{m} = \mathrm{k}_4\, G^{-0.46}$			$k_4 = 0.25$ ($\mathrm{K^{0.46}\ \mu m^{0.54}}$)		$r_4 = -0.997$	
$\lambda_\mathrm{M} = k_5\, G^{-0.47}$			$k_5 = 0.33$ ($\mathrm{K^{0.47}\ \mu m^{0.53}}$)		$r_5 = -0.997$	

through the thermocouples separated by known distances was read from data-logger record. Thus, the value of growth rate ($V = \Delta X/\Delta t$) for each sample was determined using the measured values of Δt and ΔX. The measured values of G and V are given in Table 1. More details are given in [14].

The minimum eutectic spacings, λ_m, and maximum eutectic spacings, λ_M, were measured on the longitudinal section (parallel to the pulling direction), and also average eutectic spacings, λ_L, (arithmetic average of λ_m and λ_M values) were measured from the longitudinal section. The eutectic spacings, λ_T, were measured on the transverse section (perpendicular to the pulling direction) of the samples. Approximately 20–30 λ_i (λ_L, λ_m and λ_M) values were measured for each specimen (given in Table 1).

The undercooling values, ΔT, were obtained from the detailed ΔT-λ curves, which were plotted by using experimental V and G values with the system parameters K_1, K_2.

3. Results and discussion

Al-5.7wt.%Ni eutectic samples were unidirectionally solidified with a constant V ($8.32\,\mu\mathrm{m\,s^{-1}}$) and different G (0.83–$4.02\,\mathrm{K\,mm^{-1}}$), and also with a constant G ($4.02\,\mathrm{K\,mm^{-1}}$) and different V (8.32–$483.25\,\mu\mathrm{m\,s^{-1}}$) in order to see the effect of V and G on the eutectic spacings, λ_i, and the undercooling, ΔT. As can be seen from Fig. 3 during eutectic growth, a large number of eutectic grains can be formed. All grains seemed to be oriented parallel to growth direction but usually differed in rotation about the growth axis. The normal of the α and β planes must be parallel to the polished longitudinal plane [15], however, this is not always possible. When the normals of the α and β planes are not parallel to the longitudinal plane, the eutectic spacings λ_L observed on the longitudinal plane give larger values than the eutectic spacings λ_T from the transverse polished plane. In a longitudinal view, the eutectic spacing seems to be different in each grain, because they were cut under different angles θ to the polished surface. θ values can be obtained by using the measured λ_L and λ_T values from Tables 1 and 2 ($\theta = 27.74^\mathrm{o} \pm 2.17^\mathrm{o}$). For that reason, longitudinal sections are inadequate for evaluation of the eutectic spacing without the geometrical correction. So λ_T values measured on the transverse section of the sample are more reliable. In this work, λ_T values have been compared with the similar work results and the J-H theory [16–27].

In addition to the above microstructural characteristics, several solidification faults like layer mismatches and eutectic termination were observed. As can be seen from Fig. 1b, the α-β boundary tilts toward the β lamella side and a pocked range will appear in liquid in front of the α-L interface with finally a new β lamella growing in the pocked and a positive termination forming. By this dynamic mechanism, the local spacing will decrease (λ_m). The α-β boundary tilts toward the α lamella side and the local α-L interface disappears with the lamella being overlapped by the two neighbour β lamellae (negative termination) [13]. Despite this, for microstructures that changed by positive and negative termination mechanism λ_m, λ_M values were measured as accurately as possible on each specimen.

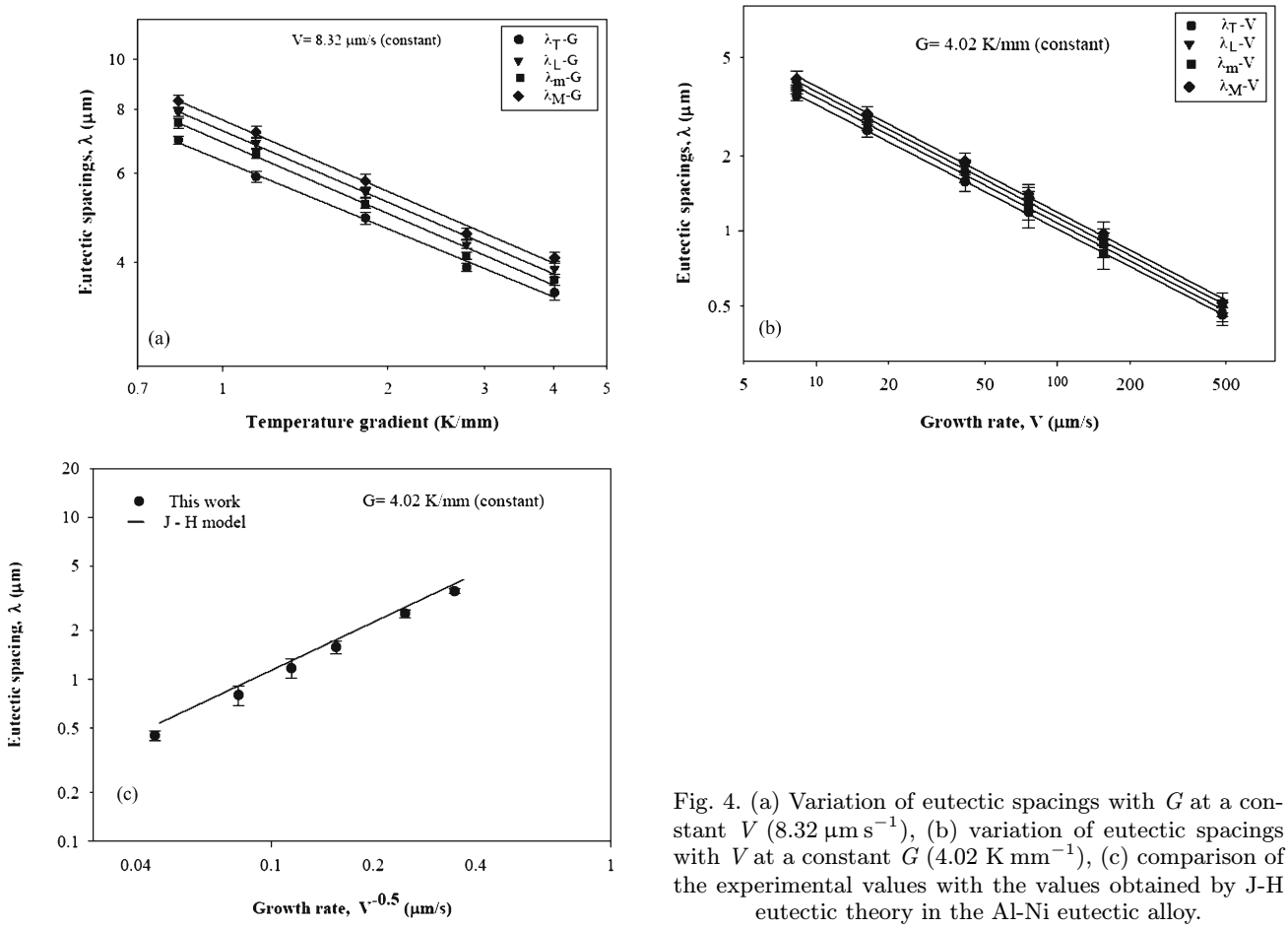

Fig. 4. (a) Variation of eutectic spacings with G at a constant V ($8.32\,\mu\mathrm{m\,s^{-1}}$), (b) variation of eutectic spacings with V at a constant G ($4.02\,\mathrm{K\,mm^{-1}}$), (c) comparison of the experimental values with the values obtained by J-H eutectic theory in the Al-Ni eutectic alloy.

Measured λ_i (λ_T, λ_L, λ_m and λ_M) are given in Table 1.

3.1. Effect of the temperature gradient and the growth rate on the eutectic spacings

The variation of the eutectic spacings, λ_i (λ_T, λ_L, λ_m and λ_M) as a function of the temperature gradients is given in Table 1 and Fig. 4a. It can be observed that an increase in the temperature gradient leads to a decrease in the eutectic spacings for a given V ($8.32\,\mu\mathrm{m\,s^{-1}}$). Thus we can describe the mathematical relationship between λ_i and G by linear regression analysis as

$$\lambda_i = k_1 G^{-m} \text{ (for the constant } V). \tag{6}$$

Dependence of λ_i (λ_T, λ_L, λ_m and λ_M) on the temperature gradient exponents was found to be 0.45, 0.47, 0.46 and 0.47, respectively.

The variation of the lamellar spacings λ_i as a function of the temperature gradient is given in Fig. 4a. It can be observed that an increase in the temperature gradient leads to a decrease in the lamellar spacings for a given constant V. The influence of temperature gradient G on λ_i has not been considered in theoretical studies for the eutectic growth. But the influence of G cannot be ignored for eutectic systems. The influence of temperature gradient on eutectic spacings was experimentally investigated by several authors [16–27].

If Eq. (6) is used in Eq. (2) and applying the condition of growth at minimum undercooling $[(\partial \Delta T/\partial G)_\mathrm{V} = 0]$ to Eq. (3) yields

$$V = \left(\frac{K_2}{K_1 k_1^2}\right) G^{2m}. \tag{7}$$

Using Eq. (7) in Eq. (2) gives

$$\Delta T = K_1' \lambda \mathrm{G}^{2m} + \frac{K_2}{\lambda}, \tag{8}$$

where $K_1' = K_2/k_1^2$. Equation (8) gives the relationship between the average undercooling ΔT, the temperature gradient G and the eutectic spacing λ_i for an isothermal solidification front. As can be seen from Eqs. (2) and (8), the temperature gradient, G, makes similar relationships with ΔT and λ as the growth

Table 2. Effect of growth rate V on the undercooling ΔT and the eutectic spacings λ_i at a constant temperature gradient G for the directionally solidified Al-Ni eutectic system, and the relationship between ΔT and V and also λ_i and V

Constant G, different V						
Solidification parameters			Microstructure parameters			
G ($\mathrm{K\,mm^{-1}}$)	V ($\mu\mathrm{m\,s^{-1}}$)	ΔT (K)	λ_T (μm)	λ_L (μm)	λ_m (μm)	λ_M (μm)
4.02	8.32	0.266	3.49 ± 0.12	3.89 ± 0.14	3.70 ± 0.09	4.08 ± 0.10
4.02	16.27	0.372	2.54 ± 0.15	2.80 ± 0.14	2.66 ± 0.13	2.95 ± 0.22
4.02	41.4	0.594	1.58 ± 0.14	1.81 ± 0.12	1.72 ± 0.15	1.90 ± 0.15
4.02	75.97	0.804	1.17 ± 0.16	1.34 ± 0.15	1.27 ± 0.17	1.41 ± 0.12
4.02	155.14	1.149	0.80 ± 0.11	0.93 ± 0.09	0.88 ± 0.10	0.97 ± 0.11
4.02	483.25	2.029	0.45 ± 0.03	0.49 ± 0.04	0.46 ± 0.05	0.51 ± 0.05

Relationships	Constant (k)	Correlation coefficients (r)
$\Delta T = k_6\ V^{0.50}$	$k_6 = 0.092$ ($\mathrm{K\,\mu m^{-0.50}\ s^{0.50}}$)	$r_6 = -0.999$
$\lambda_\mathrm{T} = k_7\ V^{-0.50}$	$k_7 = 10.76$ ($\mu\mathrm{m^{1.50}\ s^{-0.50}}$)	$r_7 = -0.998$
$\lambda_\mathrm{L} = k_8\ V^{-0.51}$	$k_8 = 11.61$ ($\mu\mathrm{m^{1.51}\ s^{-0.51}}$)	$r_8 = -0.997$
$\lambda_\mathrm{m} = k_9\ V^{-0.51}$	$k_9 = 11.04$ ($\mu\mathrm{m^{1.51}\ s^{-0.51}}$)	$r_9 = -0.997$
$\lambda_\mathrm{M} = k_{10}\ V^{-0.51}$	$k_{10} = 12.22$ ($\mu\mathrm{m^{1.51}\ s^{-0.51}}$)	$r_{10} = -0.997$

λ_T are the values of the eutectic spacing obtained from the transverse section of the samples.
λ_L are the values of the eutectic spacing obtained from the longitudinal section of the samples.
λ_m are the minimum values of the eutectic spacing obtained from the longitudinal section of the samples.
λ_M are the maximum values of the eutectic spacing obtained from the longitudinal section of the samples.

rate V. Applying the condition of growth at minimum undercooling $[(\partial\Delta T/\partial\lambda)_\mathrm{G} = 0]$ to Eq. (9) gives

$$\lambda G^m = k_2 = \mathrm{constant}_1, \tag{9a}$$

$$\frac{\Delta T}{G^m} = \frac{2K_2}{k_1} = \mathrm{constant}_2, \tag{9b}$$

$$\Delta T\lambda = 2K_2 = \mathrm{constant}_3. \tag{9c}$$

As can be seen from Eqs. (2b) and (9c), $\lambda_\mathrm{L}\Delta T$ values are exactly the same for both growth with different G at constant V and growth with different V at constant G. The relationship between λ_i and G for constant V gives similar results with the λ_i and V for constant G and also the relationship between ΔT and G is similar to the relationship between ΔT and V for both cases (Tables 1 and 2).

The exponent value of $m = 0.45$ obtained for transverse section in this work (Table 1) is in good agreement with that of 0.49 obtained by Çadırlı and Gündüz [17], but 0.45 value higher than those of 0.30, 0.33, 0.37, 0.37 and 0.28 obtained by Çadırlı et al. [18], Toloui and Hellawell [20], Gündüz et al. [16], Çadırlı et al. [19] and Kaya et al. [21] for different eutectic alloys. In the limit of the experimental uncertainties, if m is taken as 0.5, Eq. (10a) becomes $\lambda^2 G = \mathrm{constant}$. As can be seen from Table 3, an average $\lambda^2 G$ value is constant with increasing G for a constant V, and also, average $\lambda_i^2 V$ value is constant with increasing V for a constant G.

Variation in eutectic spacings λ_i with V at constant G (4.02 $\mathrm{K\,mm^{-1}}$) is given in Table 2 and shown in Fig. 4b. Variation of λ_i versus V is essentially linear on the logarithmic scale. As can be seen from Table 2 and Fig. 4b, the data form straight lines, the linear regression analysis gives the proportionality equation as

$$\lambda_i = k_2 V^{-n} \text{ (for the constant } G). \tag{10}$$

The exponent values of V for λ_i (λ_T, λ_L, λ_m and λ_M) are equal to 0.50, 0.51, 0.51 and 0.51, respectively. An average exponent value is 0.51. It is apparent that the dependence of λ_i values on the growth rate exponent (0.50) is equal to that predicted by the eutectic theory (0.50). The experimental measurements in the Al-Ni eutectic system obey the relationship $\lambda^2 V$ = constant for a given G {$\lambda_\mathrm{T}^2 V$= 101.80 $\mu\mathrm{m^3\,s^{-1}}$, $\lambda_\mathrm{L}^2 V$= 129.28 $\mu\mathrm{m^3\,s^{-1}}$, $\lambda_\mathrm{m}^2 V$= 129.28 $\mu\mathrm{m^3\,s^{-1}}$, $\lambda_\mathrm{M}^2 V$= 142.04 $\mu\mathrm{m^3\,s^{-1}}$}.

The variation of eutectic spacings as a function of the inverse square root of the growth rate is given in Fig. 4c. The experimental $\lambda_\mathrm{T}^2 V$ value (101.80 $\mu\mathrm{m^3\,s^{-1}}$) in this work is in good agreement with the result 105.88 $\mu\mathrm{m^3\ s^{-1}}$ calculated from J-H eutectic theory [8]. However, $\lambda_\mathrm{T}^2 V$ value obtained in this study is higher than those of 56.9 $\mu\mathrm{m^3\,s^{-1}}$, 59 $\mu\mathrm{m^3\,s^{-1}}$ and 65.6 $\mu\mathrm{m^3\,s^{-1}}$ reported by Mahallawy and Farag [24], Lemkey et al. [25], and Lapin [26, 27] for Al-Ni eutectic alloy, respectively. And also, experimental $\lambda_\mathrm{T}^2 V$ value

Table 3. Comparison of the experimental results with the theoretical predictions for the directionally solidified Al-Ni eutectic alloy grown for constant V

Constant V, different G						
Dependence of λ on ΔT and G						Dependence of ΔT on G
$\lambda_T \Delta T$ (K μm)	$\lambda_L \Delta T$ (K μm)	$\lambda_T^2 G$ (K μm)	$\lambda_L^2 G$ (K μm)	$\lambda_m^2 G$ (K μm)	$\lambda_M^2 G$ (K μm)	$\Delta T\ G^{-0.45}$ ($K^{1.45}$ $\mu m^{-0.45}$)
0.904	1.027	0.039	0.050	0.045	0.055	0.141
0.889	1.037	0.042	0.057	0.051	0.062	0.142
0.905	1.018	0.043	0.054	0.049	0.060	0.141
0.876	0.972	0.043	0.053	0.048	0.058	0.142
0.921	1.027	0.049	0.061	0.055	0.067	0.142
0.899 ± 0.017	**1.0162 ± 0.025**	**0.043 ± 0.0036**	**0.055 ± 0.0042**	**0.049 ± 0.0037**	**0.060 ± 0.0045**	**0.142 ± 0.0002**

$\lambda_m \Delta T = 0.966 \pm 0.025$ (constant)
$\lambda_M \Delta T = 1.067 \pm 0.026$ (constant)
$\Delta T G^{-0.45} = 0.142 \pm 0.0002$ (constant)

Table 4. Comparison of the experimental results with the theoretical predictions for the directionally solidified Al-Ni eutectic alloy grown for constant G

Constant G, different V						
Dependence of λ on ΔT and V						Dependence of ΔT on V
$\lambda_T \Delta T$ (K μm)	$\lambda_L \Delta T$ (K μm)	$\lambda_T^2 V$ ($\mu m^3\ s^{-1}$)	$\lambda_L^2 V$ ($\mu m^3\ s^{-1}$)	$\lambda_m^2 V$ ($\mu m^3\ s^{-1}$)	$\lambda_M^2 V$ ($\mu m^3\ s^{-1}$)	$\Delta T\ V^{-0.50}$ (K $\mu m^{-0.50}$ $s^{0.50}$)
0.928	1.035	101.34	125.90	113.90	138.50	0.092
0.945	1.042	104.97	127.56	115.12	141.59	0.092
0.939	1.075	103.35	135.63	122.48	149.45	0.092
0.941	1.077	104.00	136.41	122.53	151.04	0.092
0.919	1.069	99.29	134.18	120.14	145.97	0.092
0.913	0.994	97.86	116.03	102.26	125.69	0.092
0.931 ± 0.0129	**1.048 ± 0.032**	**101.80 ± 2.80**	**129.28 ± 7.81**	**116.07 ± 7.69**	**142.04 ± 9.23**	**0.092**

$\lambda_m \Delta T = 0.993 \pm 0.033$ (constant)
$\lambda_M \Delta T = 1.099 \pm 0.036$ (constant)
$\Delta T V^{-0.50} = 0.092$ (constant)

is fairly smaller than the results of 1200 $\mu m^3\ s^{-1}$ and 3300 $\mu m^3\ s^{-1}$ obtained by Hunziker and Kurz [22], Lee and Verhoeven [23] for Al-Ni alloy, respectively. These differences might be due to the different solidification condition and different composition.

3.2. Effect of temperature gradients and growth rates on the minimum undercooling

The undercooling ΔT of the solidifying eutectic was obtained from ΔT-λ curves, which were plotted by using the experimental V and G values with Eqs. (3) and (9). Figure 5a shows the relationship between ΔT and λ for the Al-Ni eutectic system at different G and constant V. As can be seen from Fig. 5a, ΔT increases with increasing G while the extreme spacing λ decreases. Although G values increased approximately 4.84 times, ΔT value increased approximately 2.03 times. Figure 5b shows the ΔT-λ curves for different V and constant G. The influence of V is certain on the eutectic spacing, λ, and ΔT. ΔT also increases with the increasing V, whereas λ decreases. Although V values increased approximately 58 times, ΔT value increased approximately 7.63 times.

Figure 6a shows the dependence of ΔT on G for a constant V. As can be seen from Tables 3 and 4 and Fig. 6a, the relationship between ΔT and G, ΔT and λ can be expressed as:

$$\Delta T = k_1 G^{0.45} \text{ (for constant } V), \quad (11a)$$

$$\Delta T \lambda_T = \text{constant}_3 \text{ (for constant } V), \quad (11b)$$

where k_1 is a constant (0.142 $K^{0.55}$ $\mu m^{0.45}$). The exponent value for G of $m = 0.45$ for the ΔT-G rela-

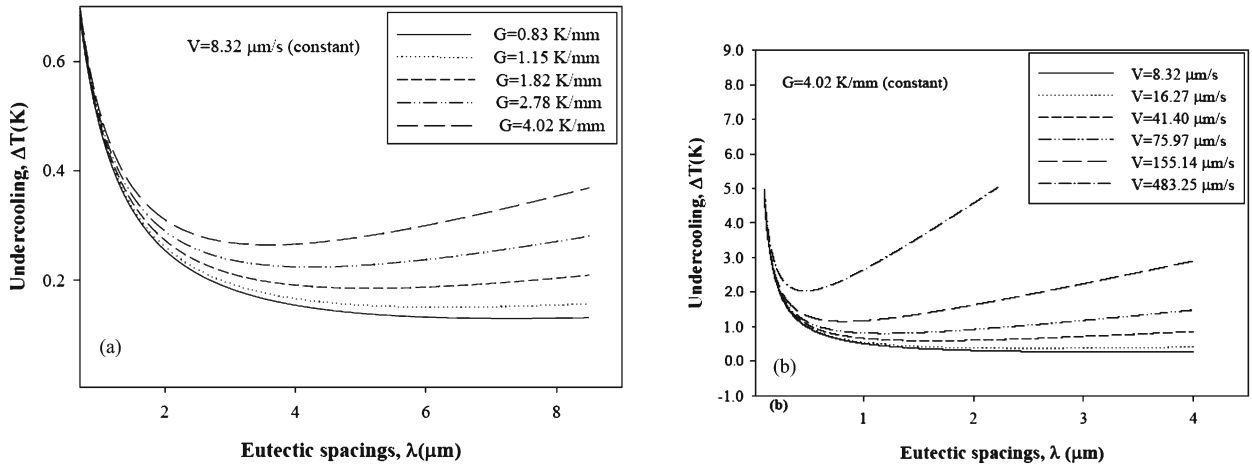

Fig. 5. Calculated average undercooling ΔT values versus eutectic spacing λ for the Al-Ni eutectic alloy (a) at a constant V ($8.32\,\mathrm{mm\,s^{-1}}$), (b) at a constant G ($4.02\,\mathrm{K\,mm^{-1}}$).

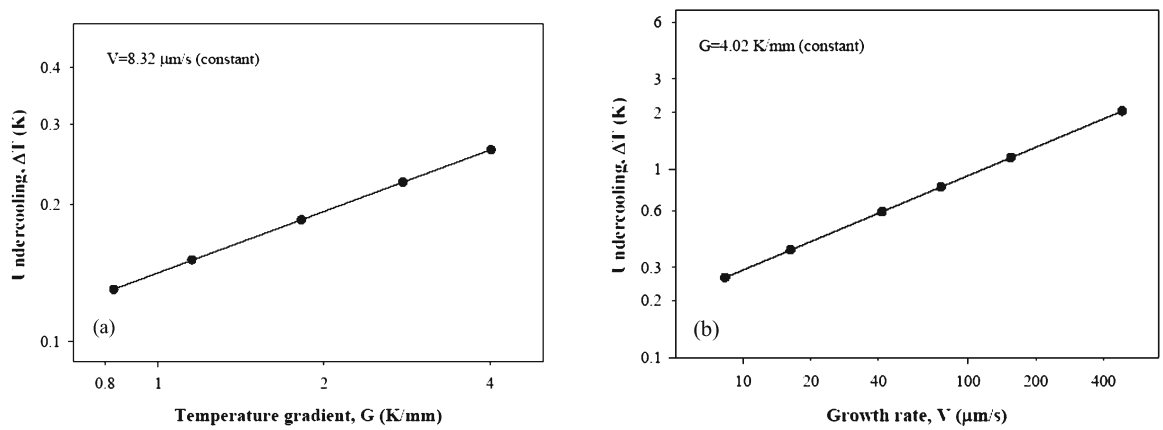

Fig. 6. (a) Variation of the minimum undercooling with G at a constant V ($8.32\,\mathrm{\mu m\,s^{-1}}$), (b) the variation of the undercooling with V at a constant G ($4.02\,\mathrm{K\,mm^{-1}}$).

tionship is equal to the exponent value of 0.45 for the λ_T-G relationship. As can be seen from Figs. 5 and 6, the temperature gradients affect the eutectic spacings and the undercoolings in the same way with the growth rates.

Figure 6b shows the variation of ΔT as a function of V for a constant G. ΔT increases with the increasing V. As can be seen from Tables 3 and 4 and Fig. 6b, the dependence of ΔT on V and λ can be given as:

$$\Delta T = k_6 V^{0.50} \text{ (for constant } G\text{)}, \quad (12a)$$

$$\Delta T \lambda_T = \text{constant}_3 \text{ (for constant } G\text{)}, \quad (12b)$$

where k_6 is a constant ($0.092\,\mathrm{K\,\mu m^{-0.50}\,s^{0.50}}$). The exponent value (0.50) is in good agreement with 0.53, 0.48, 0.50 and 0.50 obtained by Gündüz et al. [16], Çadırlı et al. [20], Kaya et al. [21] for different eutectic systems and obtained by J-H eutectic theory – Eq. (2a), respectively.

4. Conclusions

In this study, Al-5.7wt.%Ni eutectic alloy was solidified unidirectionally upwards under various solidification conditions. The microstructural features observed from the longitudinal and transverse sections of the samples studied for examining the dependence of solidification parameters (G and V) on microstructure parameters (λ_T, λ_L, λ_m and λ_M). The principal results can be summarized as follows:

1. The values of microstructure parameters decrease as the values of G and V increase. The exponent values relating to the temperature gradient (0.45–0.51) for eutectic spacings (λ_i) agree well with the previous experimental results.

2. The experimentally determined bulk growth rate $\lambda_T^2 V$ of $101.80\,\mathrm{\mu m^3\,s^{-1}}$ is very close to a theoretical value of $105.88\,\mathrm{\mu m^3\,s^{-1}}$ calculated according to the J-H model.

3. ΔT increases and λ decreases with the increasing

temperature gradient G for a given V. ΔT increases and λ decreases with the increasing growth rate V for a given G.

4. As results from experimentally measured exponent values for G and V, the effects of temperature gradient and growth rate on the eutectic spacings and the undercoolings are similar.

Acknowledgements

This project was supported by Erciyes University, Scientific Research Project Unit under Contract No: FBA--08-447. The authors are grateful to Erciyes University Scientific Research Project Unit for the financial support.

References

[1] CAHN, R. W.—SIEMERS, P. A.—GEIGER, J. E.—BARDHAN, P.: Acta Metall., *35*, 1987, p. 2737.
[2] LAPIN, J.—WIERZBINSKI, S.—PELACHOVA, T.: Intermetallics, *7*, 1999, p. 705.
[3] LAPIN, J.—PELACHOVA, T.—BAJANA, O.: Intermetallics, *8*, 2000, p. 1417.
[4] LAPIN, J.: Intermetallics, *5*, 1997, p. 615.
[5] ELLIOTT, R.: Eutectic Solidification Processing Crystalline and Glassy Alloys. Guilford, UK, Butterworths 1983.
[6] DAVIS, S. H.: Solidification Processing of Eutectic Alloys. A publication of the Metallurgical Society, Inc., Ohio 1988.
[7] STEFANESCU, D. M.—ABBASCHIAN, G. J.—BAYUZICK, R. J.: Solidification Processing of Eutectic Alloys. Warrendale, PA, Metallurgical Society of AIME 1988.
[8] JACKSON, K. A.—HUNT, J. D.: Trans. Metall. Soc. AIME, *236*, 1966, p. 1129.
[9] HUNT, J. D.: Sci. Tech. Adv. Mat., *2*, 2001, p. 147.
[10] DATYE, V.—LANGER, J. S.: Phys. Rev., *24B*, 1981, p. 4155.
[11] TRIVEDI, R.—MAGNIN, P.—KURZ, W.: Acta Metall., *35*, 1987, p. 971.
[12] TRIVEDI, R.—MASON, J. T.—VERHOEVEN, J. D.—KURZ, W.: Metall. Trans., *22A*, 1991, p. 2523.
[13] SHARMA, G.—RAMANUJAN, R. V.—TIVARI, G. P.: Acta Mater., *48*, 2000, p. 875.
[14] KAYA, H.—ÇADIRLI, E.—GÜNDÜZ, M.: Appl. Phys., *94A*, 2009, p. 155.
[15] OURDJINI, A.—LIU, J.—ELLIOTT, R.: Mater. Sci. Tech., *10*, 1994, p. 312.
[16] GÜNDÜZ, M.—KAYA, H.—ÇADIRLI, E.—ÖZMEN, A.: Mat. Sci. Eng., *369A*, 2004, p. 215.
[17] ÇADIRLI, E.—GÜNDÜZ, M.: J. Mat. Proceess. Tech., *97*, 2000, p. 74.
[18] ÇADIRLI, E.—ÜLGEN, A.—GÜNDÜZ, M.: Materials Transactions (JIM), *40*, 1999, p. 989.
[19] ÇADIRLI, E.—KAYA, H.—GÜNDÜZ, M.: Mat. Res. Bull., *38*, 2003, p. 1457.
[20] TOLOUİ, B.—HELLAWELL, A.: Acta Metall., *24*, 1976, p. 565.
[21] KAYA, H.—ÇADIRLI, E.—GÜNDÜZ, M.: J. Mat. Eng. and Perf., *12*, 2003, p. 465.
[22] HUNZIKER, O.—KURZ, W.: Acta Mater., *45*, 1997, p. 4981.
[23] LEE, J. H.—VERHOEVEN, J. D.: J. Cryst. Growth, *143*, 1994, p. 86.
[24] EL-MAHALLAWY, N. A.—FARAG, M. M.: In: Proceeding of Int. Conf. on Solidification and Casting of Metals '77. London, The Metals Society 1979, p. 106.
[25] LEMKEY, F. D.—HERTZBERG, R. W.—FORD, J. A.: Trans. TMS-AIME, *233*, 1965, p. 334.
[26] LAPIN, J.: Kovove Mater., *28*, 1990, p. 232.
[27] KOVÁČOVÁ, K.—LAPIN, J.: Kovove Mater., *28*, 1990, p. 30.
[28] MASSALSKI, T. T.: Binary Alloy Phase Diagrams. Amer. Soc. for Metals. Metals Park (Ohio) 1986, p. 140.
[29] HUNZIKER, O.—KURZ, W.: Metall. Trans., *30A*, 1999, p. 3167.

Appendix

The physical parameters used for Al-Ni eutectic alloy

Symbol	Unit	Value	References
T_E	K	912.55	[28]
m_α	K (wt.%)$^{-1}$	–2.74	[28]
m_β	K (wt.%)$^{-1}$	9.62	[28]
C_E	wt.%	5.7	[28]
C_o	wt.%	94.3	[28]
f_α	–	0.75	[23]
f_β	–	0.25	[23]
Γ_α	K μm	0.2	[22]
Γ_β	K μm	0.18	[22]
θ_α	°	29	[22]
θ_β	°	59	[22]
D	μm^2 s^{-1}	5000	[29]
K_1	K s μm^{-2}	0.0044832	calculated from the physical parameters
K_2	μm K	0.4747	calculated from the physical parameters
$\lambda^2 V = \frac{K_2}{K_1}$	μm^3 s^{-1}	105.88	calculated from the physical parameters